Switchable Metamaterial with Terahertz Buffering and Absorbing Performance

Liu, Chenxi; Xu, Yanlin; Liu, Hanqing; Lin, Mingtuan; Zha, Song

DOI
10.1109/JPHOT.2021.3107533

Publication date
2021

Document Version
Final published version

Published in
IEEE Photonics Journal

Switchable Metamaterial With Terahertz Buffering and Absorbing Performance

Chenxi Liu, Yanlin Xu, Hanqing Liu, Mingtuan Lin, and Song Zha

***Abstract*—A terahertz metamaterial with switching characteristics from optical buffering to absorbing performance is realized by incorporating a phase-change film of vanadium dioxide. By introducing the electromagnetically induced transparency behavior based on simple strip pairs, the slow light effect with group delay up to 3.5 ps is obtained. When vanadium dioxide is in the insulator state, the remarkable delay can be observed as the incident pulse transmits through the designed structure. Once the vanadium dioxide film is tuned to the metallic state, the metamaterial is switched to a terahertz absorber and the maximum absorption rate of 94% is observed at 1.04 THz. The switching mechanism is discussed by analyzing the electric field and power loss distributions, as well as the impedance matching principle. Moreover, the buffering capability and the absorption performance both remain noticeable within a wide range of the incidence angle. This work offers a strategy for the function-switching metamaterial which provides potential applications in terahertz detecting, switching and slow light devices.**

***Index Terms*—Switchable metamaterial, vanadium dioxide, buffering, absorbing.**

I. Introduction

ARTIFICIAL electromagnetic metamaterials have been intensively studied in the past decade for unique properties which cannot be found in natural material [1]–[3]. Taking advantage of geometrical scalability, scientists have demonstrated a variety of devices based on metamaterials such as filters, absorbers, and modulators in a wide electromagnetic spectrum ranging from radio to optical regimes [4]–[8]. Particularly, metamaterials proved a significant method to manipulate the propagation of the terahertz waves, which overcome the knotty restriction that few materials in nature can be employed in THz range [9]–[12]. The growth of metamaterial-based THz devices, including metasurface waveplate, high-speed modulators and high-sensitivity biosensors, promises potential applications in wireless communications, imaging, detecting, and spectroscopy [13]–[17].

For the dynamic control, active approaches have been introduced to manipulate the response spectrum in metamaterial such as PIN diodes, microelectromechanical system (MEMS), graphene, and semiconductors, etc [18]–[22]. In recent years, the phase-change material based reconfigurable metamaterials have been widely investigated. The typical phase-change materials integrated in metamaterial to realize dynamic response are GeSnTe (GST) and vanadium dioxide (VO_2) [23] –[27]. For instance, Cao *et al.* demonstrated the control of double Fano resonances with a broad spectral tunability (from 2124 nm to 3082 nm) based on GST fishnet metamaterial through switching between the amorphous and crystalline states [28]. Generally, the phase transition of VO_2 is more preferable compared with GST due to the lower critical temperature. The phase transition of VO_2 from insulator state to metallic state can be enabled thermally, electrically, and optically thus the metamaterials integrated with VO_2 layer exhibit controllable characteristics [29]–[31].

Previous works have reported that the VO_2 layer can be employed in metamaterials to tailor various performances such as filtering, absorbing, and polarization converting, while commonly the resonant frequency, bandwidth, and transmission or absorption magnitude are adjusted [32]–[39]. For example, Wu *et al.* proposed an adjustable ultra-wideband metamaterial perfect absorber based on VO_2 rings and the absorbing bandwidth of more than 90% absorptance reaches up to 3.30 THz [40]. Hu *et al.* demonstrated an electrically tunable terahertz band-pass filter by applying bias current to the VO_2 layer and the modulation depth at resonance can reach 96% [41]. Particularly, there has been growing interest in switchable metamaterials which are capable of integrating completely different functionalities into a single architecture by taking advantage of the large-scale conductivity variation of VO_2 [42]. By employing the insulator-to-metal transition of VO_2, Ding *et al.* [43] and Li *et al.* [44] proposed metasurfaces with diversified functionalities that can be switched from a broadband absorber to a reflecting plate. He *et al.* [45], Song *et al.* [46] and Zhang *et al.* [47] presented bifunctional plasmonic metasurfaces integrated with absorption and polarization-conversion capability working in different frequency region.

In this work, we present a function-switchable metamaterial achieving both terahertz buffering and high absorption by incorporating VO_2 layer, which has seldom been reported. The classic bright-bright coupling structure is employed to generate electromagnetically induced transparency (EIT) which results in prominent slow light effect. The incident Gaussian pulse can be noticeably delayed by the metamaterial compared with the bare substrate. By inducing insulator to metal transition, the buffering capability is switched to absorbing functionality while

Manuscript received June 17, 2021; revised August 11, 2021; accepted August 22, 2021. Date of publication August 27, 2021; date of current version September 15, 2021. *(Corresponding author: Yanlin Xu.)*

Chenxi Liu, Yanlin Xu, Mingtuan Lin, and Song Zha are with the College of Electronic Science, National University of Defense Technology, Changsha 410000, Hunan, China (e-mail: liuchenxi09@nudt.edu.cn; 13298656824@163.com; linmingtuan08@163.com; zhasong1987@hotmail.com).

Hanqing Liu is with the Delft University of Technology, 2628 CD Delft, The Netherlands (e-mail: h.liu-7@tudelft.nl).

Digital Object Identifier 10.1109/JPHOT.2021.3107533

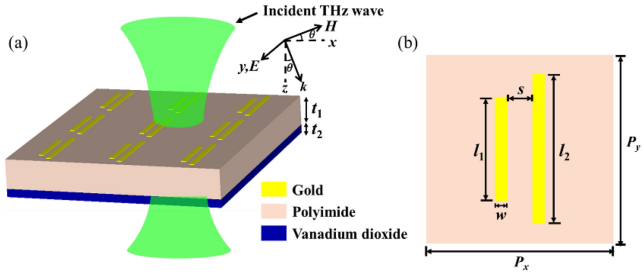

Fig. 1. (a) The perspective view of the proposed metamaterial and (b) the front view of the unit cell.

the terahertz absorption up to 0.94 at 1.04 THz is accomplished. Compared with the analysis of the switchable EIT metamaterial reported in [42], the practical function of optical buffering is investigated and demonstrated. And the classic but simple unit cell exhibits an uncomplicated geometry which is more feasible to fabricate in practice. Additionally, the proposed metamaterial exhibits stable optical buffering and absorbing performance within a wide range of incidence angles.

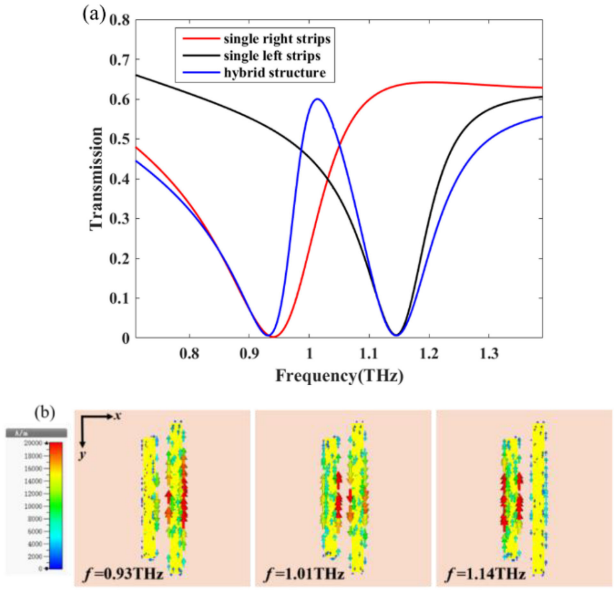

Fig. 2. (a) Transmission spectra of the single metal strip on either side of the unit and the hybrid structure (b) Surface current distributions at transmission peak and dips.

II. Structure Design and Simulation Model

A schematic diagram of the proposed metamaterial and its unit cell are depicted in Fig. 1(a) and (b). The structure consists of a stack of three layers including a patterned gold array, a polyimide substrate and a thin VO_2 film at the bottom. The periodic length of the metamaterial is $P_x = P_y = 120$ μm. The first layer is a typical EIT coupling structure which contains two gold strips serving as the bright mode resonators. The parameters of the metal strips are $l_1 = 80$ μm, $l_2 = 100$ μm, and $w = 8$ μm. The thickness of the metal layer is 0.2 μm. The separation distance between the adjacent resonators is $s = 18$ μm. The thickness of the polyimide substrate is $t_1 = 30$ μm. The dielectric constant and loss of the polyimide layer are $\varepsilon_p = 3.5$ and $\tan\delta = 0.0027$ respectively. The thickness of the VO_2 film is $t_2 = 1.0$ μm. The terahertz wave illuminates on the metamaterial with an incidence angle of θ in the xz plane.

In low THz band, the gold is considered as lossy metal with conductivity of 4.561×10^7 S/m. Generally, the varying dielectric properties of VO_2 can be acquired by the Drude model [48], which indicates nearly frequency-independent conductivity in low THz region. The relative permittivity of VO_2 in insulator state is about 12. For simplicity, the varying conductivity of the VO_2 film in different state can alternatively qualify the insulator-to-metal phase transition. In our calculations, we assume that $\sigma_{VO_2} = 200\mathrm{S/m}$ when VO_2 is in the insulator state, and $\sigma_{VO_2} = 20000\mathrm{S/m}$ when it is in the metallic state [39]. Two order of magnitude variations is relatively simple to achieve in practical experiment via various tuning methods [49], [50].

Taking the practical application into account, the fabrication procedure of our designed structure could be carried out as follows: firstly, the polyimide substrate is spin-coated with a resist which is patterned using photolithography. After development of the resist, Au layer is deposited, generating strip arrays with high aspect ratios and well-defined dimensions after removal of the resist. Subsequently, the VO_2 layer is synthesized on the bottom by magnetron sputtering technique from a pure vanadium target and an Ar/O_2 gas mixture. Finally, by applying thermal, electrical or optical stimuli, the insulator-metal transition can be induced and the actively controlled conductivity of the VO_2 layer can be realized [51]–[53].

The performance of the proposed structure is numerically calculated by the electromagnetic simulation software CST Microwave Studio based on finite element method. The unit cell boundary conditions are adopted in x and y directions to simulate the periodic structure. Initially, the electromagnetic wave illuminates perpendicularly on the metamaterial along the z direction. The transmission coefficient S_{21} and the reflection coefficient S_{11} can be calculated by the software. The absorption of the proposed EIT metamaterial can be obtained through the equation $A = 1 - |S_{21}|^2 - |S_{11}|^2$. The investigated frequency range is from 0.7 to 1.4 THz.

III. Results and Discussions

A. EIT Phenomenon and Optical Buffering Performance

To obtain the buffering performance, an EIT phenomenon is generated by a typical design consisting of strip pair array [54]. This simple strip array is utilized here to achieve a rather uncomplicated design of bifunctional metamaterial compared with previous works. The transmission spectra of the single metal strip on either side of the unit and the hybrid structure with VO_2 film in insulator phase are depicted in Fig. 2(a). The single metal strip on either side of the unit exhibits evident transmission dip at different resonant frequency, indicating prominent radiative mode. As the strips are assembled in the same structure, the transparency window appears at the frequency between two original transmission dips. Fig. 2(b) indicates the surface current

distributions of the hybrid structure at transmission peak and dips. The strips with lengths of 80 μm and 100 μm are excited strongly at 1.14 THz and 0.93 THz respectively. At 1.01 THz, the strips on both sides are simultaneously evoked due to resonance detuning, and the excited surface currents on two strips are almost antiphase. This leads to the destructive interference of the radiative fields, which consequently results in the transparency peak. Apparently, in the generation of the transparency window, the thin VO_2 film serves as a general dielectric which has little influence on EIT behavior.

The coupled oscillator model is employed to further investigate the EIT effect [55]–[57]. Since the EIT effect in our work is induced by bright-bright coupling between two detuned electric dipole resonators, generally the radiative two particle model can be employed to illustrate the coupling mechanism. This model is described analytically by the following equations [55].

$$\begin{cases} \ddot{p}_1(t) + \gamma_1 \dot{p}_1(t) + {\omega_1}^2 p_1(t) - k^2 \exp(i\varphi) p_2(t) = f_1(t) \\ \ddot{p}_2(t) + \gamma_2 \dot{p}_2(t) + {\omega_2}^2 p_2(t) - k^2 \exp(i\varphi) p_1(t) = f_2(t) \end{cases} \tag{1}$$

Where (ω_1, ω_2) and (γ_1, γ_2) represent the resonance frequencies and damping rates of the two radiative excitation particles $(p_1(t), \mathrm{p}_2(t))$respectively. $k^2 \exp(i\varphi)$ is the complex coupling coefficient and φ is the phase shift between two particles. The coupled particles are subjected to the external force $f_1(t)$ and$f_2(t)$. For simplicity, the circumstance of normal incidence is assumed and the discussion is restricted to the case that $\varphi = 0$ and $f_1(t) = f_2(t)$. This assumption is reasonable as the phase shift stemming from retardation effect can be neglected under normal incidence. Therefore the different part of the metamaterial suffered the same external electromagnetic field. By assuming a solution $p_1(t) = P_1 \exp(-i\omega t)$, $p_2(t) = P_2 \exp(-i\omega t)$ and $f(t) = \tilde{f} \exp(-i\omega t)$, the above coupled equations can be solved by

$$P_1 = \frac{k^2 + (\omega_2^2 - \omega^2 - i\omega\gamma_2)}{(\omega_1^2 - \omega^2 - i\omega\gamma_1)(\omega_2^2 - \omega^2 - i\omega\gamma_2) - k^4} \tilde{f} \tag{2}$$

$$P_2 = \frac{k^2 + (\omega_1^2 - \omega^2 - i\omega\gamma_1)}{(\omega_1^2 - \omega^2 - i\omega\gamma_1)(\omega_2^2 - \omega^2 - i\omega\gamma_2) - k^4} \tilde{f} \tag{3}$$

Treating the proposed design as a thin film, the current density J of the metamaterial can be described as: $J = -n_s\omega(P_1 + P_2) = \sigma_e E_s$, where σ_e is the surface conductivity, n_s represents the averaged electron density, and E_s denotes the spatially averaged electric field on the sheet. Assuming $\tilde{f} = CE_s$, we obtained

$$\sigma_e = -Cn_s\omega \frac{2k^2 + (\omega_1^2 - \omega^2 - i\omega\gamma_1) + (\omega_2^2 - \omega^2 - i\omega\gamma_2)}{(\omega_1^2 - \omega^2 - i\omega\gamma_1)(\omega_2^2 - \omega^2 - i\omega\gamma_2) - k^4} \tag{4}$$

C is the proportionality constant. Hence, the scattering parameters can be obtained by considering the metamaterial as two-dimensional sheet with the surface conductivity:

$$R = \frac{-Z_0\sigma_{se}}{2 + Z_0\sigma_{se}}, \quad T = \frac{2}{2 + Z_0\sigma_{se}} \tag{5}$$

where Z_0 is the impedance of the incident waves. By fitting with the EIT spectra in Fig. 2(a), the parameters in the coupled oscillation model can be obtained. Fig. 3 shows

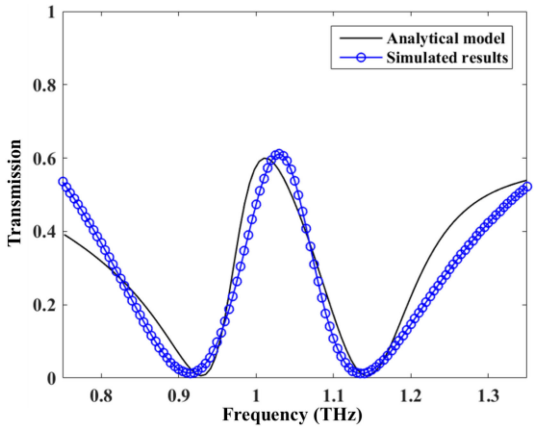

Fig. 3. The simulated EIT spectra and the fitted curve based on analytical model.

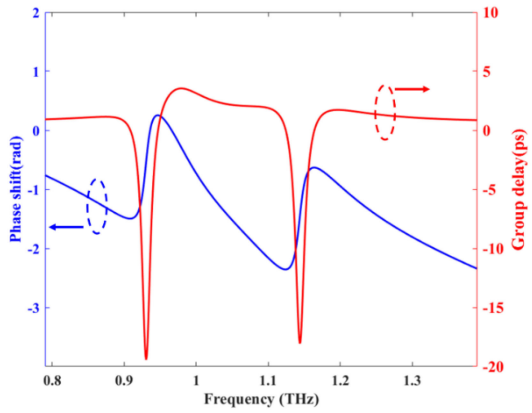

Fig. 4. Phase shift and group delay spectra as the incident wave transmits through the proposed structure when VO_2 is in the insulator state.

the fitted EIT curve based on analytical model, which exhibits good agreement with the simulated results. This result verifies the validity of the coupled oscillation model. The corresponding fitting parameters of the analytical models are$\gamma_1 = 0.19\mathrm{rad/ps}, \gamma_2 = 0.18\mathrm{rad/ps}, k = 0.1\mathrm{rad/ps}$. The nearly equivalent damping rates of two radiative particles manifest similar resonance strength of the electric dipole evoked by metal strips, which coincides with the resonance curve depicted in Fig. 2(a). It is worthy to note that the value of the coupling coefficient is rather small. This result is consistent with the plasmon-hybridation-scheme, in which the better transparency window is attributed to weaker hybridization.

A remarkable feature of the EIT phenomenon is the strong phase dispersion which manifests noticeable slow light effect. The terahertz buffering performance accompanying with the EIT phenomenon is investigated. The group delay is a significant index which is used to measure the velocity retardation of the terahertz wave transmitting through the metamaterial. Generally, the group delay can be calculated by $\tau = -\mathrm{d}\phi/\mathrm{d}\omega$, where ϕ is the transmission phase shift. Fig. 4 shows the transmission phase shift and the group delay spectra of the proposed metamaterial. Evidently, a sharp slope of the phase shift can be observed while

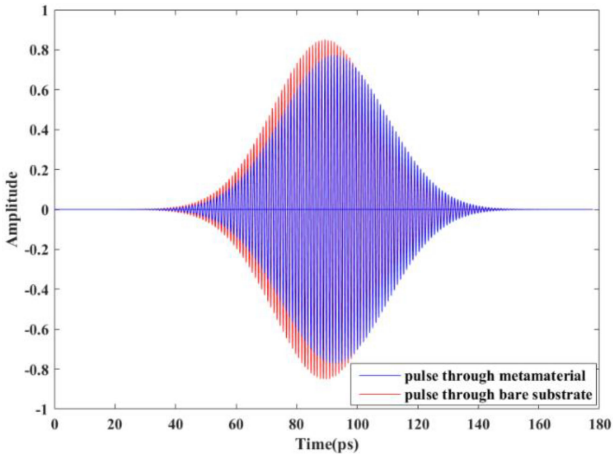

Fig. 5. The waveform recorded by the electric filed probe when the Gaussian pulse propagates normally through the metamaterial (blue curve) and the bare substrate (red curve).

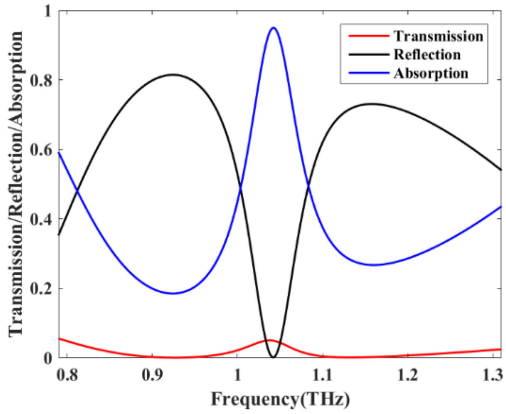

Fig. 6. Transmission, reflection, and absorption spectra of the hybrid metamaterial when the VO_2 film is in the metallic state.

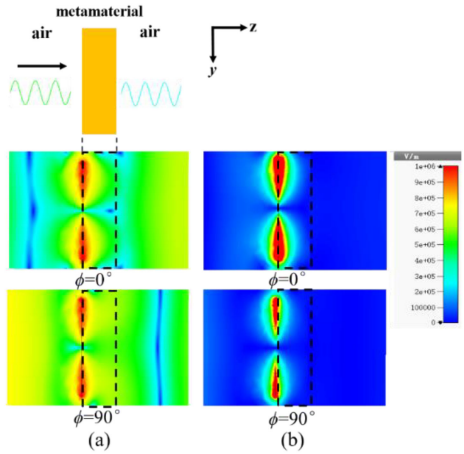

Fig. 7. Cross section of the electric field distribution at 1.04 THz as the phase of incident wave rises from 0° to 90° when the VO_2 film is (a) in the insulator state and (b) in the metallic state respectively.

a region of the positive group delay is realized in the vicinity of the transparency window. A maximum value of 3.5 ps can be obtained at 0.98 THz. Therefore, a high performance of terahertz buffering capability is fulfilled simultaneously with the EIT effect.

To demonstrate the terahertz buffering capability of the proposed metamaterial, we simulate a situation where a Gaussian pulse centered at 0.98 THz propagates normally through the designed structure [58]. The planewave with *y*-polarization is set in the *z*-axis direction as the excitation source. The periodic boundary conditions are used in *x*- and *y*- directions. The electric field probe is placed behind the metamaterial to record the transmitted terahertz wave for transient analysis. For comparison, the same signal is simulated to transmit through the bare substrate. Fig. 5 shows the transmitted pulse waveform recorded by the electric field probe. It can be observed that the peak of the transmitted pulse locates at 89 ps as the incident wave propagates normally through the bare substrate. Whereas the peak of the transmitted pulse emerges at 92 ps as the incident wave propagates through the metamaterial. The incident Gaussian pulse is delayed by approximately 3 ps by the designed metamaterial, which coincides with the results in Fig. 4. Thus, the incident terahertz wave can be effectively buffered. In addition, it is worthy to note that the peak amplitude and the pulse width of the transmitted wave through the metamaterial is slightly different compared with that through the bare substrate, which can be attributed to the dispersion feature of the metamaterial.

B. Switchable Characteristics and Absorption Capability

As mentioned above, the proposed structure turns to a terahertz absorber as the VO_2 film undergoes phase transition to the metallic state. Fig. 6 represents the transmission, reflection and absorption spectra of the metamaterial under normal incidence as the VO_2 film turns to the metal phase. It can be seen that the incident wave almost cannot be transmitted in the investigated frequency region. The increasing conductivity of VO_2 film dramatically depresses the terahertz transmission. Meanwhile, a reflection dip simultaneously with an absorption peak appears at 1.04 THz. The maximum absorption reaches up to 94% under normal incidence and the relative bandwidth of 90% absorption is 5%. Therefore, the switchable function between terahertz buffering and absorbing is accomplished with the insulator–metallic phase transition of VO_2. Interestingly, we can find that the shape of the transmission window remains unchanged despite of the rapid decreasing magnitude. This phenomenon can be explained that the destructive interference still occurs though the intensity of the radiative field is weakened.

To have a deep insight into the switching mechanism, the electric field distribution of the structure is further investigated at 1.04 THz with different phase state of the VO_2 film. Fig. 7(a) depicts the sectional view of the field distributions along with the propagation direction as the phase of the incident wave increases from 0° to 90° when the VO_2 film is in the insulator state. As can be seen, the incident wave moves from one side of the hybrid metamaterial to the other side with slight intensity attenuation. By contrast, when the VO_2 film is in metallic state, the electric

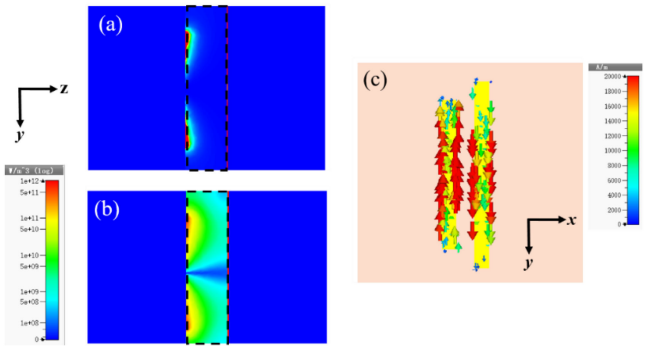

Fig. 8. Cross section of the power loss density at 1.04 THz when the VO_2 film is in (a) the insulator state and (b) the metallic state respectively. (c) Top view of the surface current distribution on the metal layer at 1.04 THz when the metamaterial behaves as an absorber.

field locates mainly on the metamaterial while the radiative field and transmitted field in the free space are both weakened as can be found from Fig. 7(b). In addition, the intensity of the field distribution on the metamaterial manifests a pronounced distinction compared with the field intensity in the free space.

For deeper understanding of the absorption mechanism, the power loss density at 1.04THz is calculated as shown in Fig. 8(a) and (b). An unambiguous concentration of power loss can be found in the whole metamaterial observed from Fig. 8(b) when VO_2 is in the metal phase, which is distinctive with the circumstance when VO_2 is in the insulator phase as shown in Fig. 8(a). As the VO_2 turns more metallic, the multiple reflections between the metal resonators and the bottom film cause the prominent transmission loss in the lossy metal and dielectric, which consequently leads to the evident absorption behavior. Meanwhile, we calculate and plot the top view of the surface current distribution in Fig. 8(c) when VO_2 is in the metallic state. Compared with the current distributions at transparency peak in Fig. 2(b), it is interesting to note that the similar antiphase distributions can be observed when the metamaterial behaves as an absorber. The destructive interference still occurs regardless of the weakened electromagnetic energy caused by the variations of the VO_2 conductivity. This well explains the maintained EIT window in the transmission spectrum despite the low transmission rate observed in Fig. 6.

The absorption performance is further investigated by employing the impedance matching principle. The designed metamaterial is considered as an isotropic uniform medium characterized with effective impedance Z_{eff} normalized to the value of vacuum. The effective impedance can be obtained through the S-parameter retrieved method described as:

$$Z_{\text{eff}} = \sqrt{\frac{\eta}{\varepsilon}} = \sqrt{\frac{(1+S_{11})^2 - S_{21}^2}{(1-S_{11})^2 - S_{21}^2}} \tag{6}$$

The real and imaginary parts of the effective impedance as a function of frequency when VO_2 is in different state are calculated and plotted in Fig. 9(a) and (b). When VO_2 is in the metal phase, it is observed from Fig. 9(a) that the real part approaches to 1 and the imaginary part is close to 0 around 1.04 THz, which

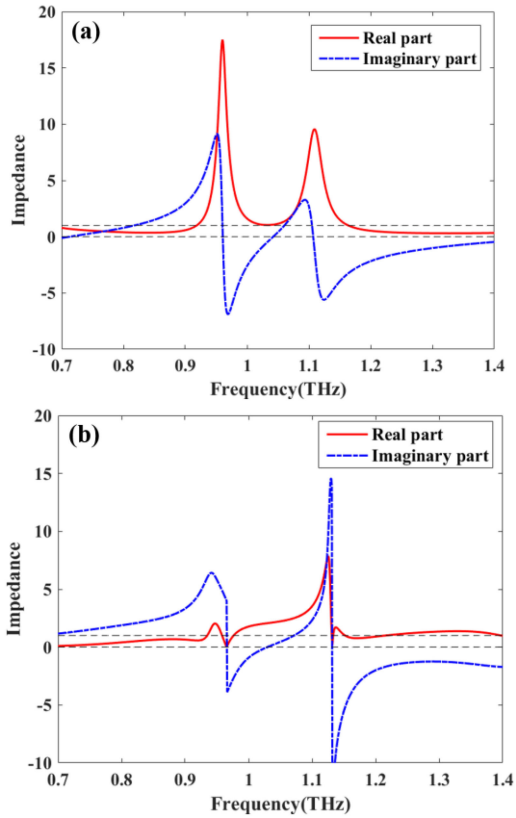

Fig. 9. Real and imaginary parts of the retrieved effective impedance when the VO_2 film is in (a) the metallic state and (b) the insulator state respectively.

indicates impedance match between the metamaterial and the free space. Thus, the reflection is minimized and the absorption peak is achieved. Whereas when the VO_2 is in the insulator state, the absorption condition cannot be matched as shown in Fig. 9(b).

C. *Parameter Analysis*

Following the above discussions, the dependence of the buffering and absorbing performance on the thickness of the polyimide dielectric h is investigated. Fig. 10(a) and (b) depict the group delay with VO_2 in insulator state and the absorption spectra with VO_2 in metallic state as a function of h. It is noticed from Fig. 10(a) that the maximum value of the group delay appears at different position, which indicates that the slow light region can be customized by adjusting the dielectric thickness. The absorption behavior when VO_2 is in metallic state manifests evident dependence on the dielectric thickness. As shown in Fig. 10(b), the absorption peak displays red shift with the increasing h. With the rising thickness of the substrate, the resonant frequencies caused by the metal strip array are changed owing to the increased propagation length of the transmitted wave in the dielectric. We note that a rapid decrease of the absorption peak can be found as $h = 15$ μm. The impedance mismatch between the free space and the metamaterial results in strong reflection. Moreover, the relatively shorter distance

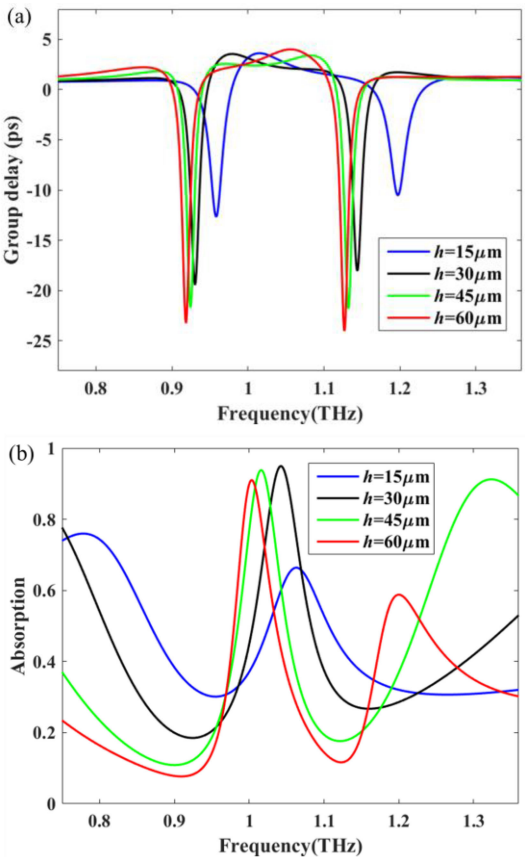

Fig. 10. (a) The group delay and (b) the absorption spectra as a function of h when VO_2 is in the insulator and metallic state respectively.

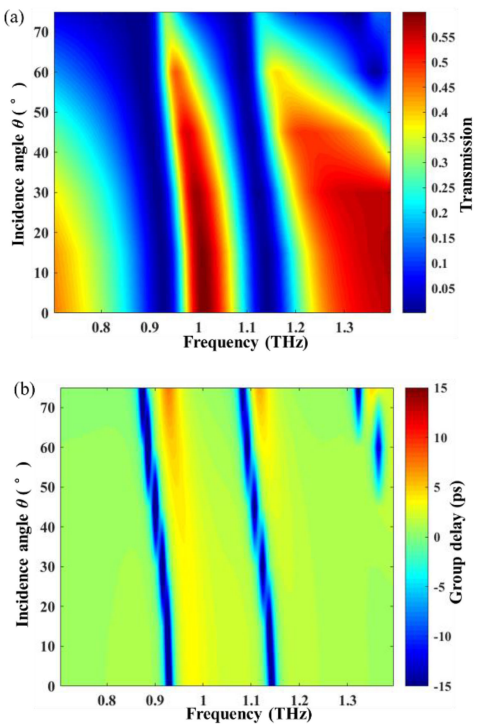

Fig. 11. The dependence of (a) the EIT curve and (b) corresponding group delay spectra on the incidence angle θ.

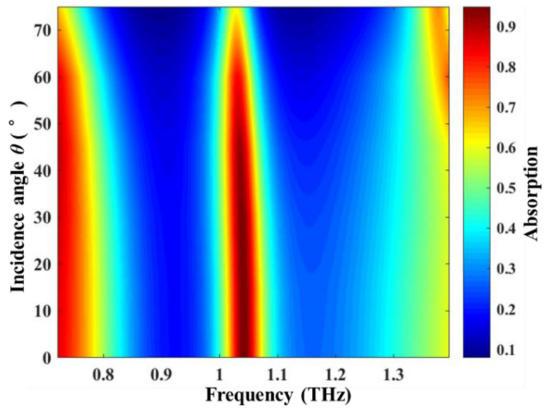

Fig. 12. The dependence of the absorption spectra on the incidence angle θ.

leads to the lower power loss and the electromagnetic energy cannot be confined as before.

For realistic applications, the influence of the illumination direction is an important index that should be considered. Fig. 11(a) and (b) depict the variations of the EIT window and the accompanying group delay with the incidence angle θ increasing from 0° to 75°, when VO_2 is in the insulator state. It can be seen from the evolution contour figure that the EIT window exhibits a red shift and shows an excellent stability until the incidence angle is over 60°. The transparency peak manifests a sharp decrease at $\theta = 75°$. Nevertheless, the group delay remains relatively large value at $\theta = 75°$ which indicates more stable behavior of the terahertz buffering capability. The maximum value of the group delay is 3.5 ps at $\theta = 0°$ and it changes to 7.3 ps at $\theta = 75°$. Thus, the prominent slow light effect is well maintained. Fig. 12 reveals the dependence of the absorption spectra on the incidence angle when VO_2 is in the metallic state. The position of the absorption peak is almost invariable. The maximum absorption falls down less than 90% when the incidence angle is up to 60°, and then decreases rapidly as θ increases further. Therefore, the incidence angle-roust feature can be obtained in both terahertz buffering and absorbing state of the metamaterial.

IV. Conclusion

In summary, a switchable metamaterial with optical buffering and absorbing functionalities is proposed and numerically investigated in terahertz range. The evident slow light effect is achieved accompanying with the EIT phenomenon based on bright-bright mode coupling. The coupled oscillation model is used to analyze the mechanism of the EIT effect. The noticeable delay can be observed as the incident pulse transmits through the proposed metamaterial. By enabling the insulator-to-metal transition of the incorporated phase-change film, the buffering performance can be switched to the pronounced absorbing behavior. The electric field and power loss distributions are calculated to explore the switching mechanism, and the influence of the thickness of the dielectric is also analyzed. Furthermore, the buffering capability and the absorbing performance can sustain over a wide range of the incidence angle. Consisting

of a classic but simple EIT structure and a thin layer of VO_2 material, the presented design has an uncomplicated geometry and is easy to be integrated with other terahertz devices. The proposed metamaterial may provide potential applications in a wide range such as optical buffering, sensing, detecting, and switching.

REFERENCES

[1] R. A. Shelby, D. R. Smith, and S. Schultz, "Experimental verification of a negative index of refraction," *Science*, vol. 292, no. 6, pp. 77–79, Apr. 2001.

[2] A. J. Hoffman *et al.*, "Negative refraction in semiconductor metamaterials," *Nat. Mater.*, vol. 6, pp. 946–950, Oct. 2007.

[3] A. Alu and N. Engheta, "Guided modes in a waveguide filled with a pair of single-negative (SNG), double-negative (DNG), and/or double-positive (DPS) layers," *IEEE Trans. Micro. Theory*, vol. 52, no. 1, pp. 199–210, Jan. 2004.

[4] F. Ding, Y. Cui, X. Ge, Y. Jin, and S. He, "Ultra-broadband microwave metamaterial absorber," *Appl. Phys. Lett.*, vol. 100, no. 10, Dec. 2012, Art. no. 103506.

[5] F. Alves, D. Grbovic, B. Kearney, N. V. Lavrik, and G. Karunasiri, "Bi-material terahertz sensors using metamaterial structures," *Opt. Exp.*, vol. 21, no. 11, pp. 13256–13271, Jun. 2013.

[6] D. Schurig *et al.*, "Metamaterial electromagnetic cloak at microwave frequencies," *Science*, vol. 314, no. 5801, pp. 977–980, Nov. 2006.

[7] M. Zhang and Z. Song, "Terahertz bifunctional absorber based on a graphene-spacer-vanadium dioxide-spacer-metal configuration," *Opt. Exp.*, vol. 28, no. 8, pp. 11780–11788, Apr. 2020.

[8] W. Zhu, I. D. Rukhlenko, and M. Premaratne, "Graphene metamaterial for optical reflection modulation," *Appl. Phys. Lett.*, vol. 102, Jun. 2013, Art. no. 241914.

[9] C. Du *et al.*, "An ultra-broadband terahertz metamaterial coherent absorber using multilayer electric ring resonator structures based on anti-reflection coating," *Nanoscale*, vol. 12, pp. 9769–9775, Apr. 2020.

[10] S. Xiao, T. Wang, T. Liu, X. Yan, Z. Li, and C. Xu, "Active modulation of electromagnetically induced transparency analogue in terahertz hybrid metal-graphene metamaterials," *Carbon*, vol. 126, pp. 271–278, Oct. 2018.

[11] Y. Huang *et al.*, "Tunable circular polarization conversion and asymmetric transmission of planar chiral graphene-metamaterial in terahertz region," *Carbon*, vol. 119, pp. 305–313, Apr. 2017.

[12] J. Gu *et al.*, "Active control of electromagnetically induced transparency analogue in terahertz metamaterials," *Nat. Commun.*, vol. 3, Oct. 2012, Art. no. 1151.

[13] D. Wang, S. Sun, Z. Feng, W. Tan, and C. Qiu, "Multipolar-interference-assisted terahertz waveplates via all-dielectric metamaterials," *Appl. Phys. Lett.*, vol. 113, no. 20, Nov. 2018, Art. no. 201103.

[14] D. Hu *et al.*, "Dispersion characteristic of ultrathin terahertz planar lenses based on metasurface," *Opt. Commun.*, vol. 322, pp. 164–168, Jul. 2014.

[15] Y. Wang *et al.*, "Tunable bandwidth of double electromagnetic induced transparency windows in terahertz graphene metamaterial," *RSC Adv,* vol. 8, no. 65, pp. 37057–37063, Jun. 2018.

[16] L. Xie, W. Gao, J. Shu, Y. Ying, and J. Kono, "Extraordinary sensitivity enhancement by metasurfaces in terahertz detection of antibiotics," *Sci. Rep.*, vol. 5, Mar. 2015, Art. no. 8671.

[17] S. Xiao *et al.*, "Tunable anisotropic absorption in hyperbolic metamaterials based on black phosphorous/dielectric multilayer structures," *J. Lightw. Technol.*, vol. 37, no. 13, pp. 3290–3297, Jul. 2019.

[18] S. Izadshenas, A. Zakery, and Z. Vafapour, "Tunable slow light in graphene metamaterial in a broad terahertz range," *Plasmonics*, vol. 13, pp. 63–70, Feb. 2018.

[19] Y. Fan *et al.*, "A metamaterial modulator based on electrically controllable electromagnetically induced transparency," *Sci. Rep.*, vol. 7, Jan. 2017, Art. no. 40441.

[20] P. Pitchappa, M. Manjappa, C. P. Ho, R. Singh, N. Singh, and C. K. Lee, "Active control of electromagnetically induced transparency analog in terahertz MEMS metamaterial," *Adv. Opt. Mater.*, vol. 4, pp. 541–547, Apr. 2016.

[21] P. Q. Liu *et al.*, "Highly tunable hybrid metamaterials employing split-ring resonators strongly coupled to graphene surface plasmons," *Nat. Commun.*, vol. 6, Nov. 2015, Art. no. 8969.

[22] H. T. Chen, W. J. Padilla, J. M. O. Zide, A. C. Gossard, A. J. Taylor, and R. D. Averitt, "Active terahertz metamaterial devices," *Nature*, vol. 444, no. 7119, pp. 597–600, Nov. 2006.

[23] G. C. Carrillo, G. R. Nash, H. Hayat, M. J. Cryan, and C. D. Wright, "Design of practicable phase-change metadevices for near-infrared absorber and modulator applications," *Opt. Exp.*, vol. 24, no. 12, pp. 13563–13573, Jun. 2016.

[24] T. Cao, C. W. Wei, R. E. Simpson, L. Zhang, and M. J. Cryan, "Broadband polarization-independent perfect absorber using a phase-change metamaterial at visible frequencies," *Sci. Rep.*, vol. 4, Feb. 2014, Art. no. 3955.

[25] M. Hashemi, S. H. Yang, T. Wang, N. Sepúlveda, and M. Jarrahi, "Electronically-controlled beam-steering through vanadium dioxide metasurfaces," *Sci. Rep.*, vol. 6, Oct. 2016, Art. no. 35439.

[26] L. Liu, L. Kang, T. S. Mayer, and D. H. Werner, "Hybrid metamaterials for electrically triggered multifunctional control," *Nat. Commun.*, vol. 7, Art. no. 13236, Oct. 2016.

[27] W. Zhu, R. Yang, Y. Fan, Q. Fu, and F. Zhang, "Controlling optical polarization conversion with $Ge_2Sb_2Te_5$-based phase-change dielectric metamaterials," *Nanoscale*, vol. 10, no. 25, pp. 12054–12061, May 2018.

[28] T. Cao, C. Wei, R. E. Simpson, L. Zhang, and M. J. Cryan, "Fast tuning of double fano resonance using a phase-change metamaterial under low power intensity," *Sci. Rep.*, vol. 4, Mar. 2014, Art. no. 4463.

[29] M. M. Qazilbash *et al.*, "Mott transition in vO_2 revealed by infrared spectroscopy and nano-imaging," *Science*, vol. 318, pp. 1750–1753, Jan. 2017.

[30] X. Duan, S. Chen, H. Cheng, Z. Li, and J. Tian, "Dynamically tunable plasmonically induced transparency by planar hybrid metamaterial," *Opt. Lett.*, vol. 38, no. 4, pp. 483–485, Feb. 2013.

[31] T. L. Cocker *et al.*, "Phase diagram of the ultrafast photoinduced insulator-metal transition in vanadium dioxide," *Phys. Rev. B*, vol. 85, no. 15, Apr. 2012, Art. no. 155120.

[32] H. Zhu *et al.*, "Continuously tuning the impedance matching at the broadband terahertz frequency range in vO_2 thin film," *Opt. Mater. Exp.*, vol. 9, no. 1, pp. 315–329, Jan. 2019.

[33] Z. Song, K. Wang, J. Li, and Q. Liu, "Broadband tunable terahertz absorber based on vanadium dioxide metamaterials," *Opt. Exp.*, vol. 26, no. 6, pp. 7148–7154, Mar. 2018.

[34] L. Chen and Z. Song, "Simultaneous realizations of absorber and transparent conducting metal in a single metamaterial," *Opt. Exp.*, vol. 28, no. 5, pp. 6565–6571, Mar. 2020.

[35] Z. Song, Y. Deng, Y. Zhou, and Z. Liu, "Terahertz toroidal metamaterial with tunable properties," *Opt. Exp.,* vol. 27, no. 4, pp. 5792–5797, Feb. 2019.

[36] Q. Chu, Z. Song, and Q. Liu, "Omnidirectional tunable terahertz analog of electromagnetically induced transparency realized by isotropic vanadium dioxide metasurfaces," *Appl. Phys. Exp.*, vol. 11, no. 8, Jul. 2018, Art. no. 082203.

[37] Z. Song, M. Wei, Z. Wang, G. Cai, Y. Liu, and Y. Zhou, "Terahertz absorber with reconfigurable bandwidth based on isotropic vanadium dioxide metasurfaces," *IEEE Photon. J.*, vol. 11, no. 2, Apr. 2019, Art. no. 4600607.

[38] Z. Song, Y. Deng, Y. Zhou, and Z. Liu, "Tunable toroidal dipolar resonance for terahertz wave enabled by a vanadium dioxide metamaterial," *IEEE Photon. J.*, vol. 11, no. 2, Apr. 2019, Art. no. 4600705.

[39] T. Lv *et al.*, "Hybrid metamaterial switching for manipulating chirality based on vO_2 phase transition," *Sci. Rep.*, vol. 6, Mar. 2016, Art. no. 23186.

[40] G. Wu, X. Jiao, Y. Wang, Z. Zhao, Y. Wang, and J. Liu, "Ultra-wideband tunable metamaterial perfect absorber based on vanadium dioxide," *Opt. Exp.*, vol. 29, no.no. 2, pp. 2703–2711, Jan. 2021.

[41] F. Hu *et al.*, "Electrically triggered tunable terahertz band-pass filter based on vO_2 hybrid metamaterial," *IEEE J. Sel. Top. Quant.*, vol. 25, no. 3, May/Jun. 2018, Art. no. 4700207.

[42] Z. Song, A. Chen, J. Zhang, and J. Wang, "Integrated metamaterial with functionalities of absorption and electromagnetically induced transparency," *Opt. Exp.*, vol. 27, no. 18, pp. 25196–25204, Sep. 2019.

[43] F. Ding, S. Zhong, and S. I. Bozhevolnyi, "Vanadium dioxide integrated metasurfaces with switchable functionalities at terahertz frequencies," *Adv. Opt. Mater.*, vol. 6, no. 9, Feb. 2018, Art. no. 1701204.

[44] X. Li *et al.*, "Switchable multifunctional terahertz metasurfaces employing vanadium dioxide," *Sci. Rep.*, vol. 9, Apr. 2019, Art. no. 5454.

[45] H. He *et al.*, "Thermally switchable bifunctional plasmonic metasurface for perfect absorption and polarization conversion based on vO_2," *Opt. Exp.*, vol. 28, no. 4, pp. 4563–4570, Feb. 2020.

[46] Z. Song and J. Zhang, "Achieving broadband absorption and polarization conversion with a vanadium dioxide metasurface in the same terahertz frequencies," *Opt. Exp.*, vol. 28, no. 8, pp. 12487–12497, Apr. 2020.

[47] M. Zhang, J. Zhang, A. Chen, and Z. Song, "Vanadium dioxide-based bifunctional metamaterial for terahertz waves," *IEEE Photon. J.*, vol. 12, no. 1, Feb. 2020, Art no. 4600109.

[48] P. U. Jepsen *et al.*, "Metal-insulator phase transition in a vO_2 thin film observed with terahertz spectroscopy," *Phys. Rev. B*, vol. 74, no. 20, Nov. 2006, Art. no. 205103.

[49] M. Nakajima, N. Takubo, Z. Hiroi, Y. Ueda, and T. Suemoto, "Photo-induced insulator-metal phase transition observed by the terahertz pump-probe spectroscopy," *Ultrafast Phenomena Semiconductors Nanostructure Mater. XIII*, vol. 7214, Feb. 2009, Art. no. 72140Q.

[50] S. D. Ha, Y. Zhou, C. J. Fisher, S. Ramanathan, and J. P. Treadway, "Electrical switching dynamics and broadband microwave characteristics of vO_2 radio frequency devices," *J. Appl. Phys.*, vol. 113, no.no. 18, Jun. 2013, Art. no. 184501.

[51] M. T. Nouman, J. Hwang, M. Faiyaz, G. Lee, D. Y. Noh, and J. H. Jang, "Dynamic-metasurface-based cavity structures for enhanced absorption and phase modulation," *ACS Photon,* vol. 6, no. 2, pp. 374–381, Dec. 2018.

[52] Y. Zhao, Q. Huang, H. Cai, X. Lin, and Y. Lu, "A broadband and switchable vO_2-based perfect absorber at the THz frequency," *Opt. Commun.*, vol. 426, pp. 443–449, Jun. 2018.

[53] G. Zhang, H. Ma, C. Lan, R. Gao, and J. Zhou, "Microwave tunable metamaterial based on semiconductor-to-metal phase transition," *Sci. Rep.*, vol. 7, Jul. 2017, Art. no. 5773.

[54] X. R. Jin *et al.*, "Highly-dispersive transparency at optical frequencies in planar metamaterials based on two-bright-mode coupling," *Opt. Exp.*, vol. 19, no. 22, pp. 21652–21657, Oct. 2011.

[55] X. Hu *et al.*, "Plasmon induced transparency and absorption in bright-bright mode coupling metamaterials: A radiating two-oscillator model analysis," *J. Phys. D Appl. Phys.*, vol. 50, no. 2, Nov. 2017, Art. no. 025301.

[56] X. He *et al.*, "Implementation of selective controlling electromagnetically induced transparency in terahertz graphene metamaterial," *Carbon*, vol. 123, pp. 668–675, Aug. 2017.

[57] R. Yahiaoui *et al.*, "Electromagnetically induced transparency control in terahertz metasurfaces based on bright-bright mode coupling," *Phys. Rev. B*, vol. 97, no. 15, Apr. 2018, Art. no. 155403.

[58] F. Y. Meng, Q. Wu, D. Erni, K. Wu, and J. C. Lee, "Polarization-independent metamaterial analog of electromagnetically induced transparency for a refractive-index-based sensor," *IEEE Trans. Microw. Theory Tech.*, vol. 60, no. 10, pp. 3013–3022, Oct. 2012.